



Cite this: *Chem. Sci.*, 2025, **16**, 15997

All publication charges for this article have been paid for by the Royal Society of Chemistry

Received 3rd June 2025
Accepted 30th July 2025

DOI: 10.1039/d5sc04058b
rsc.li/chemical-science

Introduction

The coordination environment around a metal center plays a crucial role in influencing molecular transition metal chemistry. Thus, ligand design has been recognized as one of the main pathways to modulate the reactivity of metal centers. Traditionally, supporting ligands are utilized to influence the electronics and sterics of a metal complex. Phosphines represent the classical type of such L-type behavior, with their wide range of electronic and steric tunability influencing the metal center while remaining chemically “innocent” spectators as they tend to avoid direct participation in substrate transformations.¹

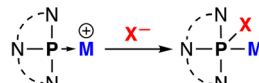
In the past few decades, an opposite, “non-innocent” behavior of ligands has attracted increased attention in coordination chemistry and catalysis. Several classes of participatory ligand transformations have been identified, such as redox-active and cooperative ligands.^{2,3} As a subclass of the latter, Z-type acceptor ligands have risen to prominence, featuring interactions between the metal and Lewis acidic boron, aluminum, gallium, antimony, and tellurium centers.^{4–6}

In this vein, rare reports of participatory behavior of neutral phosphine ligands have emerged, including the formation of metallophosphoranes as intermediates in a range of processes, for example in M–F/P–R exchange reactions as well as

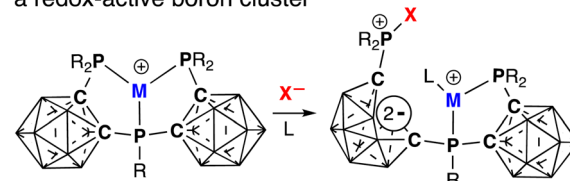
phosphine-assisted C–F bond activation.⁷ Recently, nontrigonal constrained trivalent phosphorus compounds, which are ambiphilic at the P center, have been demonstrated to exhibit remarkable non-spectator behavior in their metal complexes, adding anionic ligands to the phosphorus atom and converting to five-coordinate metallophosphoranes (Scheme 1).^{8–11}

We and others have been interested in the redox-active behavior of boron clusters and its utilization in metal-free bond activation, electrochemistry, and coordination chemistry.^{12–17} Polyhedral carborane clusters have been employed in catalysis, luminescent materials, medicinal chemistry, crystal engineering, polymeric materials, and energy

Previous work: nonspectator behavior of neutral ambiphilic non-trigonal phosphines



This work: nonspectator behavior of neutral trigonal phosphines driven by a redox-active boron cluster



Scheme 1 Non-spectator behavior of trivalent phosphine ligands in metal complexes.

Department of Chemistry and Biochemistry, University of South Carolina, 631 Sumter St., Columbia, South Carolina 29208, USA. E-mail: perlyshkov@sc.edu

† These authors contributed equally to this work.



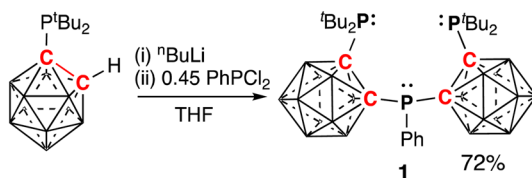
storage.^{18–26} In the realm of ligand design, the unusual electronic and steric properties of cluster-based ligands have been used to impart novel or enhanced reactivity in metal complexes.^{27–31} The redox activity of twelve-vertex $\{C_2B_{10}\}$ cages, specifically their two-electron reduction transforming the neutral *clos*- $\{C_2B_{10}\}$ cluster to the dianionic open *nido*- $\{C_2B_{10}\}^{2-}$ cluster, has been employed to stabilize low-valent main group centers as well as to drive changes in the bite angle and coordination ability of the ligands.^{32–35}

Herein, we describe the first example of nontraditional ligation involving a redox-active carboranyl phosphine complex of copper(I), wherein the electron-donating pyramidal trivalent phosphorus center serves as a binding site for nucleophilic chloride and azide anions (Scheme 1). The resulting zwitterionic complexes feature cationic copper and phosphonium centers and the dianionic open *nido*- $\{C_2B_{10}\}^{2-}$ cluster. We provide direct spectroscopic and crystallographic observations of the non-spectator phosphorus ligand behavior with either endogenous or exogenous nucleophile anions. In the case of chloride, its binding to either metal center or the phosphorus center is reversible and can be switched depending on the solvent. The reported ligand-destination coordination mode represents a new type of ambiphilicity that is driven by an internal redox event of the boron cluster imparting an electrophilic behavior on an otherwise “normal”, non-constrained electron-donating phosphine group.

Results and discussion

To capitalize on the potential redox behavior of a carboranyl phosphine system, we designed a tricoordinate ligand containing one central phosphine bridging two boron clusters with two flanking phosphines at the remaining carbon atoms of the clusters. The synthesis of the ligand involves the deprotonation of a carboranyl monophosphine $1\text{-P}^t\text{Bu}_2\text{-}o\text{-C}_2\text{B}_{10}\text{H}_{11}$ and the subsequent reaction with dichlorophenylphosphine (PhPCl_2) (Scheme 2). The target dicarboranyl triphosphine $^{7\text{Bu}}\text{P}\text{-}clos\text{-}\{C_2\text{B}_{10}\}\text{-}^{7\text{Ph}}\text{P}\text{-}clos\text{-}\{C_2\text{B}_{10}\}\text{-}^{7\text{Bu}}\text{P}$ (**1**) was isolated as a yellow powder in 72% yield (Scheme 2). The $^{31}\text{P}\{^1\text{H}\}$ NMR spectrum of **1** exhibits a characteristic, effectively AX_2 pattern with an insignificant second order effect contribution consisting of a triplet at 17.9 ppm and a doublet at 69.7 ppm with integral intensities in a 1:2 ratio. The phosphorus nuclei are strongly coupled to each other with $^{3}J_{\text{PP}} = 100$ Hz.

Yellow single crystals of **1** were grown from a dioxane solution. Single crystal X-ray diffraction confirmed the expected



Scheme 2 Synthesis of dicarboranyl triphosphine ligand $^{7\text{Bu}}\text{P}\text{-}clos\text{-}\{C_2\text{B}_{10}\}\text{-}^{7\text{Ph}}\text{P}\text{-}clos\text{-}\{C_2\text{B}_{10}\}\text{-}^{7\text{Bu}}\text{P}$ (**1**). Unlabeled cluster vertices represent BH units.

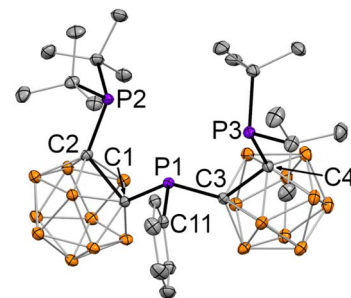


Fig. 1 The displacement ellipsoid plot (50% probability) of **1**. Hydrogen atoms are not shown.

molecular structure (Fig. 1). The ligand possesses idealized C_s symmetry with intracage C-C bonds being close (C1–C2 distance is 1.885(2) Å and C3–C4 distance is 1.842(2) Å). Similarly, corresponding C-P distances are comparable with a C2–P2 bond length of 1.903(2) Å and a C4–P3 bond length of 1.912(2) Å for the terminal phosphines, and a C1–P1 distance of 1.881(2) Å and a C3–P1 distance of 1.893(2) Å for the bridging central phosphine. The P1–C11 bond (1.831(2) Å) from the central phosphine to the phenyl ring is slightly shorter in comparison. In the crystal, the molecule adopts a conformation where the two clusters are tilted relative to each other with a torsion angle C2–C1–C3–C4 of 44.3(2)°.

Neutral *clos*- $\{C_2B_{10}\}$ cages can accept a total of two electrons and undergo significant structural rearrangement converting to open dianionic *nido*- $\{C_2B_{10}\}^{2-}$ clusters.³⁶ The potentials for the addition of two electrons are often unresolved, and, as the reduction is accompanied by an extensive bond-breaking and making transformation within the cluster, electrochemical reversibility is not observed in many instances.³⁷ As compound **1** contains two clusters bridged by the central phosphorus atom, a more complex behavior can be expected. The cyclic voltammogram of **1** in THF has three partially overlapping quasi-reversible reduction events at $E_{\text{pc}} = -1.69$ V, -2.27 V, and -3.27 V as well as returning oxidation events at $E_{\text{pa}} = -2.52$ V, -1.72 V, and -1.08 V vs. $\text{Fc}^{+/\text{0}}$, indicating the involvement of both clusters and hinting at the possibility for chemically reversible redox behavior (see SI for details).

Compound **1** bears a resemblance to a class of tridentate “PPP” phosphine ligands with a general formula $\text{PR}_2\text{-C}_6\text{H}_4\text{-P(R)-C}_6\text{H}_4\text{-PR}'_2$, where R and R' are alkyl, or,

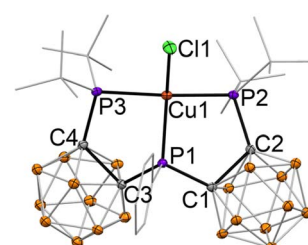


Fig. 2 The displacement ellipsoid plot (50% probability) of **1**· CuCl . Hydrogen atoms and alkyl groups of the ligand are not shown.

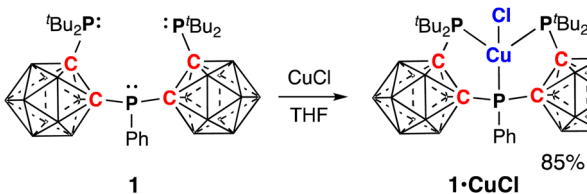


more commonly, aryl groups.^{38–40} These are strongly chelating triphosphines with a number of corresponding metal complexes, predominantly monomeric, reported.^{41–45} Thus, we sought to probe the coordination chemistry of **1** bearing in mind its increased steric profile and potential redox properties that set it apart from the arene-based analogs.

The reaction of **1** and CuCl in THF at room temperature resulted in the formation of a single product, according to the ^{31}P NMR spectrum of the reaction mixture (Scheme 3). The product maintained the AX_2 splitting pattern of the ligand with changes in the chemical shifts of the triplet (7.9 ppm) and the doublet (68.3 ppm). The signals were broadened in comparison with those of **1** and exhibited similar coupling (${}^3J_{\text{PP}} = 130$ Hz). In the ^1H NMR spectrum, the signals from the phenyl group become inequivalent, indicating arrested rotation around its C-P bond.

Dark-red single crystals of the product were grown by slow evaporation of a THF solution. The X-ray diffraction experiment revealed the expected structure of the monomeric copper(I) chloride complex $[{}^{Bu}P-closo-\{C_2B_{10}\}-{}^{Ph}P-closo-\{C_2B_{10}\}-{}^{Bu}P]CuCl$ (**1·CuCl**, Fig. 2). The metal center adopts a distorted tetrahedral geometry with three coordinated phosphines and the chloride ligand ($P1-Cu1-Cl1$ angle is $123.5(1)^\circ$ and $P3-Cu1-P2$ angle is rather large at $140.8(1)^\circ$, $\tau_4 = 0.68$). The metal-ligand distance is shorter for the central phosphine ($Cu1-P1 = 2.271(1)$ Å) in comparison with the flanking phosphines ($Cu1-P2 = 2.387(1)$ Å and $Cu1-P3 = 2.404(1)$ Å). Bite angles for the chelating five-membered rings are $P1-Cu1-P2 = 91.9(1)^\circ$ and $P2-Cu1-P3 = 97.7(1)^\circ$. Complexation to the metal brought only slight changes in the cluster geometry, most notably, the carbon–carbon bonds became longer ($C1-C2 = 1.869(2)$ Å and $C3-C4 = 1.904(2)$ Å) than in the parent **1**. The bond distances to the phosphine substituents are $C1-P1 = 1.891(1)$ Å, $C3-P1 = 1.858(1)$ Å, $C2-P2 = 1.903(1)$ Å, and $C4-P3 = 1.911(1)$ Å. The boron cages in the complex are aligned with a dihedral angle $C2-C1-C3-C4$ of $30.1(1)^\circ$.

Addition of acetonitrile to a solution of **1·CuCl** in THF brought a drastic change in its $^{31}\text{P}\{^1\text{H}\}$ NMR spectrum. Instead of the AX_2 pattern of **1·CuCl**, two doublets and one singlet in a 1:1:1 integral ratio appeared. The singlet signal is shifted significantly downfield (121.4 ppm) relative to the other two doublets at 25.3 ppm and 49.3 ppm. The change in the splitting pattern indicated that only two phosphorus nuclei remained coupled to each other ($^3J_{\text{PP}} = 166$ Hz) and that one phosphine center was no longer adjacent to the central $\text{P}(\text{Ph})$ group. This observation suggested a redox-driven boron cage opening,



Scheme 3 Synthesis of [¹¹³BuP-closo-{C₂B₁₀}-³¹PhP-closo-{C₂B₁₀}-¹¹³BuP]CuCl (1·CuCl). Unlabeled cluster vertices represent BH units.

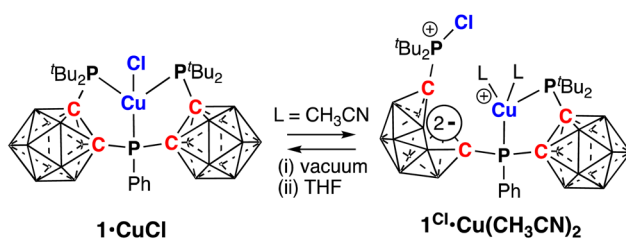
wherein the transformation from a neutral *clos*- to a dianionic *nido*-cluster proceeds with the cleavage of its C–C bond, thus separating phosphine substituents by five bonds instead of three bonds (Scheme 4).

The golden yellow single crystals of a new product were grown from its acetonitrile solution. The X-ray diffraction experiment confirmed the NMR data-based conjecture and revealed the structure of the $[{}^{\text{f}}\text{BuP}(\text{Cl})\text{-}nido\text{-}\{\text{C}_2\text{B}_{10}\}]^{\text{-}}\text{PhP-clos}\text{-}\{\text{C}_2\text{B}_{10}\}]^{\text{-}}\text{PhP}^{\text{f}}\text{Bu}_2\text{Cu}(\text{CH}_3\text{CN})_2$ complex ($1^{\text{Cl}}\cdot\text{Cu}(\text{CH}_3\text{CN})_2$, Fig. 3). The most striking structural feature of $1^{\text{Cl}}\cdot\text{Cu}(\text{CH}_3\text{CN})_2$ is the presence of one open *nido*- $\{\text{C}_2\text{B}_{10}\}$ cluster with the phosphonium group bound to the chloride anion: $\text{P}(\text{Cl})^{\text{-}}\text{Bu}_2$. The second boron cage remained in the *clos*-form and its $\text{P}^{\text{f}}\text{Bu}_2$ and central PPh_3 groups were bound to the copper center. Two acetonitrile ligands were also bound to copper. Thus, the complex $1^{\text{Cl}}\cdot\text{Cu}(\text{CH}_3\text{CN})_2$ can be formulated as a zwitterion with the di-anionic *nido*- $\{\text{C}_2\text{B}_{10}\}^{2-}$ cluster, the phosphonium cation, and the cationic copper(1) center.

The structural metrics of $1^{\text{Cl}} \cdot \text{Cu}(\text{CH}_3\text{CN})_2$ differ significantly from those of $1 \cdot \text{CuCl}$. First, the intracluster C–C bond is broken in the open cluster (C3···C4 distance of 2.925(2) Å) and the C–C bond of the remaining closed cluster C1–C2 bond compressed to 1.811(2) Å. The carbon–phosphorus bonds for the *closo*-cluster in $1^{\text{Cl}} \cdot \text{Cu}(\text{CH}_3\text{CN})_2$ are essentially identical to those in $1 \cdot \text{CuCl}$ (C1–P1 distance is 1.912(1) Å and C2–P2 is 1.906(1) Å). However, for the *nido*-cluster, the C–P bond lengths are significantly shorter with a C3–P1 distance for the central phosphine of 1.789(1) Å and, more dramatically so, for the C4–P3 bond of 1.740(1) Å to the phosphonium center. The shorter bonds for the *nido*-cluster substituents suggest of a prominent C=P double bond character typical for ylides. The P–Cl bond length is 2.024(1) Å.

The copper center in $1^{\text{Cl}}\cdot\text{Cu}(\text{CH}_3\text{CN})_2$ is in a distorted tetrahedral coordination environment with an N1–Cu1–N2 angle of $91.7(1)^\circ$ and a ligand bite angle P1–Cu1–P2 of $99.1(1)^\circ$. The Cu–P1 bond length for the central phosphine of $2.277(1)$ Å is similar to that in $1\cdot\text{CuCl}$, while the Cu–P2 bond length of $2.254(1)$ Å of the flanking phosphine became shorter.

Removal of acetonitrile from the solution of $\mathbf{1}^{\text{Cl}} \cdot \text{Cu}(\text{CH}_3\text{CN})_2$ under vacuum and re-dissolution of the residue in THF regenerated complex $\mathbf{1} \cdot \text{CuCl}$ according to ^{31}P NMR spectra (Fig. 4). Thus, in the absence of a coordinating acetonitrile solvent, the chloride ligand is transferred back to the copper center, and the boron cluster is reverted to the neutral *cis*-form.



Scheme 4 Formation of $[{}^{113}\text{BuP}(\text{Cl})-\text{nido-}\{\text{C}_2\text{B}_{10}\}-\text{PhP-closo-}\{\text{C}_2\text{B}_{10}\}-{}^{113}\text{BuP}]|\text{Cu}(\text{CH}_3\text{CN})_2$ (**1**^{Cl}). Unlabeled cluster vertices represent BH units.

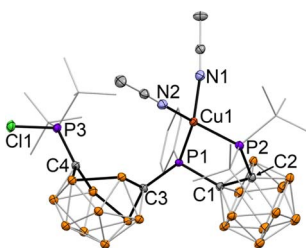


Fig. 3 The displacement ellipsoid plot (50% probability) of $1^{\text{Cl}}\cdot\text{Cu}(\text{CH}_3\text{CN})_2$. Hydrogen atoms and alkyl groups of the ligand are not shown.

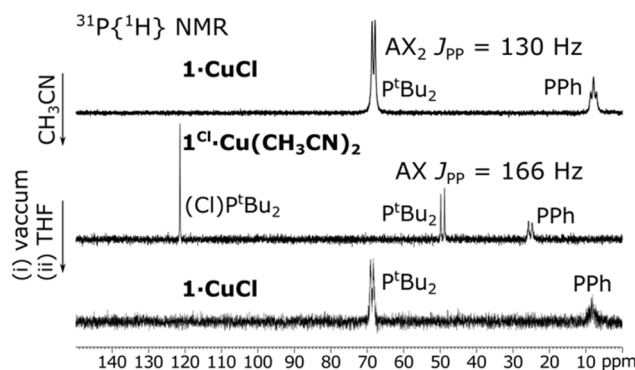


Fig. 4 Reversibility of chloride coordination to a metal center or a phosphorus center in the copper(I) complexes of 1. (top): the $^{31}\text{P}\{^1\text{H}\}$ NMR spectrum of $1\cdot\text{CuCl}$ in THF; (middle) the $^{31}\text{P}\{^1\text{H}\}$ NMR spectrum of $1\cdot\text{CuCl}$ followed by the addition of acetonitrile producing $1^{\text{Cl}}\cdot\text{Cu}(\text{CH}_3\text{CN})_2$; (bottom) the $^{31}\text{P}\{^1\text{H}\}$ NMR spectrum of $1^{\text{Cl}}\cdot\text{Cu}(\text{CH}_3\text{CN})_2$ after the removal of acetonitrile and re-dissolution of the residue in THF regenerating $1\cdot\text{CuCl}$.

The reversible transformation of $1\cdot\text{CuCl}$ to $1^{\text{Cl}}\cdot\text{Cu}(\text{CH}_3\text{CN})_2$ generating the cationic metal center through the removal of the anionic chloride ligand by the L-type coordinated neutral phosphine donor is remarkable in coordination chemistry. Examples of the formation of zwitterionic complexes by ionization of M-X bonds by ambiphilic ligands with Z-type strongly Lewis acidic backbones have been reported. Boron, aluminum, gallium, and antimony-based systems have been demonstrated to drive the transfer of halides, hydrides, alkyl, and aryl groups from coordinated metal centers, in most cases with the formation of -ate complexes.^{46–52} In addition, the non-innocent behavior of anionic phosphide ligands, often coupled with metal oxidation state change, has been shown.^{53–56}

In contrast, the abstraction of a nucleophilic anion by a neutral electron donating ligand group, such as the phosphines in 1, is rare. As mentioned in the introduction, the relevant examples include the unusual behavior of the non-trigonal neutral trivalent phosphorus compounds. The ambiphilicity of the phosphorus center has been recently demonstrated to result in the simultaneous coordination to a metal and the capability of strong binding of hydride, fluoride, or alkoxide ligands converting to metallophosphoranes.^{8–10} Additionally, similar in the outcome but mechanistically

divergent, the conversion of neutral phosphine ligands to arylphosphonium cations during the reductive elimination from a metal center has been shown for nickel, palladium, copper, and, recently, gold complexes.^{57–62}

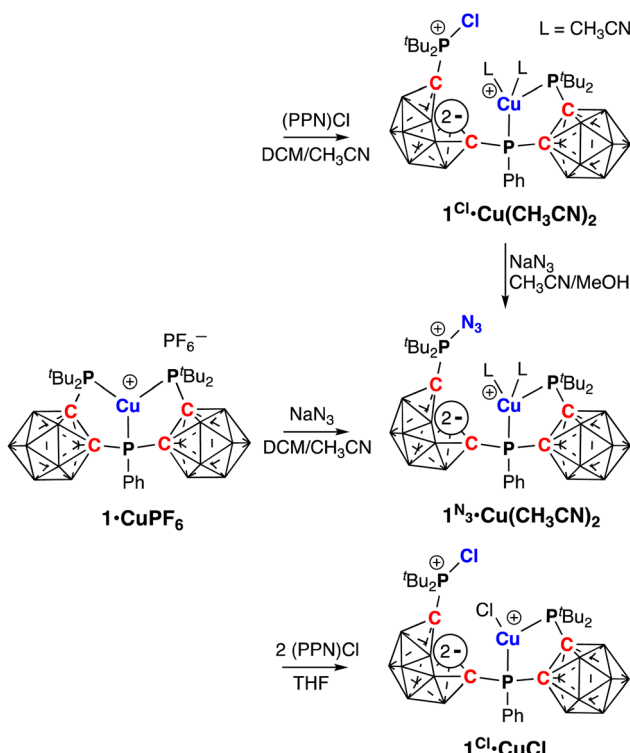
The transformation reported herein is patently different from the important examples listed above. In our case, the process is driven by the propensity of the redox-active *closo*- $\{\text{C}_2\text{B}_{10}\}$ cage to accept two electrons, thus converting the electron-rich phosphine to the phosphonium cation and generating a cationic copper(I) center. The redox activity of the complex is centered not at the metal nor at the phosphorus atom, but in the boron cluster. This cluster-driven ambiphilic behavior of 1 bears an analogy to the metal-free bond activation chemistry driven by the reduction of the boron cage in carboranyl diphosphines that has been previously reported.^{63–67}

To further explore the ambiphilic behavior of the ligand in the copper complex $1\cdot\text{CuCl}$, we have synthesized its cationic analog $1\cdot\text{CuPF}_6$ starting from $[\text{Cu}(\text{CH}_3\text{CN})_4]\text{PF}_6$. The ^{31}P NMR spectrum of $1\cdot\text{CuPF}_6$ exhibited a doublet at 74.0 ppm and a triplet at 16.3 ppm ($^3J_{\text{PP}} = 100$ Hz). This AX_2 pattern indicates that both clusters in $1\cdot\text{CuPF}_6$ are in the *closo*-form and all three phosphines are coordinated to the metal center. We have not been able to obtain single crystals of $1\cdot\text{CuPF}_6$, but instead crystallized its significantly less soluble analog with a tetraphenylborate anion, $1\cdot\text{CuBP}_4$. In its crystal structure, both clusters of the ligand are in the expected *closo*-form with the three phosphines coordinated in a distorted T-shaped arrangement around the copper cation (see SI for details). The tetraphenylborate anion does not exhibit any interaction with the metal center.

The addition of (PPN)Cl (PPN = bis(triphenylphosphine) iminium) to a solution of $1\cdot\text{CuPF}_6$ in acetonitrile generated $1^{\text{Cl}}\cdot\text{Cu}(\text{CH}_3\text{CN})_2$ according to ^{31}P NMR spectroscopy, confirming the importance of the more nucleophilic chloride for the cluster rearrangement and demonstrating that the carboranyl phosphine ligand (and not the metal center) serves as a coordination site for the exogenous chloride anion (Scheme 5). This behavior can be altered by the change of the solvent. An analogous reaction between 1 equiv. of (PPN)Cl and $1\cdot\text{CuPF}_6$ in THF generates $1\cdot\text{CuCl}$ with its PPP-ligand in the closed neutral form and the chloride bound to the metal. However, further reaction of (PPN)Cl with $1\cdot\text{CuCl}$ in THF triggers cluster opening and binding of the additional chloride to the phosphorus center forming $1^{\text{Cl}}\cdot\text{CuCl}$.

Similarly, the addition of sodium azide to a solution of $1\cdot\text{CuPF}_6$ in an acetonitrile/DCM solvent mixture resulted in a change of the ^{31}P NMR spectrum to one singlet at 80.9 ppm and a set of two doublets at 26.4 ppm and 50.4 ($^3J_{\text{PP}} = 163$ Hz), thus indicating the opening of one of the boron clusters (Scheme 5). The molecular structure of the product was confirmed by single X-ray diffraction (Fig. 5). In the resulting zwitterionic complex ${}^{[\text{Bu}]\text{P}(\text{N}_3)\text{-}nido\text{-}\{\text{C}_2\text{B}_{10}\}\text{-}^{\text{Ph}}\text{P}\text{-}closo\text{-}\{\text{C}_2\text{B}_{10}\}\text{-}^{[\text{Bu}]\text{P}}}\text{Cu}(\text{CH}_3\text{CN})_2$ ($1^{\text{N}_3}\cdot\text{Cu}(\text{CH}_3\text{CN})_2$), the azide anion is bound to the phosphorus center of the open *nido*-cluster instead of to the metal, analogously to the structure of complex $1^{\text{Cl}}\cdot\text{Cu}(\text{CH}_3\text{CN})_2$. The structural metrics of $1^{\text{N}_3}\cdot\text{Cu}(\text{CH}_3\text{CN})_2$ are largely similar to those of $1^{\text{Cl}}\cdot\text{Cu}(\text{CH}_3\text{CN})_2$. The metal-ligand





Scheme 5 Ligand-centered reactivity of $^{13}\text{B}\text{-P-closo-}\{\text{C}_2\text{B}_{10}\}\text{-}^{31}\text{P-closo-}\{\text{C}_2\text{B}_{10}\}\text{-}^{13}\text{B}\text{-P}\text{[CuPF}_6\text{]}$ (1-CuPF_6) with chloride and azide anions. Unlabeled cluster vertices represent BH units.

linearity, with an N3–N4–N5 angle of $171.3(2)^\circ$. The N3–N4 bond length is $1.233(2)$ Å, and the N4–N5 bond length is $1.124(2)$ Å, which is typical for an azide group. The P3–N3–N4 angle is $126.0(1)^\circ$.

The formation of $1^{N_3}\text{-Cu}(\text{CH}_3\text{CN})_2$ further highlights the cluster-driven ambiphilicity of the redox-active ligand **1**. The addition of the exogenous nucleophilic azide anion results in its binding to a phosphorus center of the ligand and reductive opening of the carborane cage even in competition with the available metal center. It is important to note that this behavior is triggered by the change of the solvent from weaker coordinating THF to stronger coordinating CH_3CN , which certainly provides additional stabilization to the newly formed cationic copper(I) center.

This remarkable divergence highlights the unusual coordination chemistry that is enforced by the redox-active carboranyl phosphine ligand, thus representing a new type of ambiphilic behavior that is not centered at a single atom (as, for example, in non-trigonal phosphines), but requires the cooperation of the whole molecule. Notably, the copper oxidation state does not change in all complexes described herein and it is possible that a redox-inactive metal would behave similarly. The switching of the ligand mode type from a Lewis base to the Lewis acid in the response to the changes in the coordination environment at the metal center is reminiscent to the recently reported L/Z amphotericism of carbenium fragments in rhodium complexes as well as allosteric switching in complexes with redox-active hemilabile ligands utilizing weak-link approach.^{69–72}

Conclusions

In summary, we report a new concept of ligand ambiphilicity that, instead of the employment of a Lewis acidic backbone or the redox behavior of a single center in a ligand, relies on the redox behavior of the boron cluster scaffold. The interconversion of the neutral tricoordinate and zwitterionic dicoordinate forms of the PPP-type carboranyl phosphine **1** occurs in the response to the change of a solvent and is associated with the transfer of an anionic ligand between the metal and the phosphorus center driven by reductive opening of the boron cage. Such dynamic systems enforced by ambiphilic redox-active ligands offer new possibilities for changing the coordination environment and reactivity of a metal center, and open new perspectives in catalysis.

Author contributions

Riffle, Jowers, and Luna designed experiments and carried out spectroscopic and synthetic work. Smith carried out crystal structure determination and analysis. Peryshkov conceptualized the project, provided guidance, and acquired funding. All authors contributed to the writing and editing of the manuscript.

Conflicts of interest

There are no conflicts to declare.

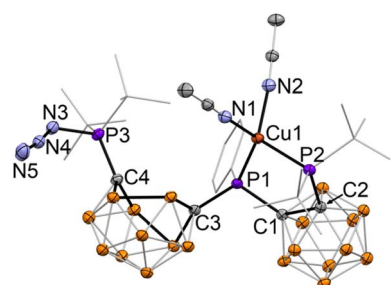


Fig. 5 The displacement ellipsoid plot (50% probability) of $1^{N_3}\text{-Cu}(\text{CH}_3\text{CN})_2$. Hydrogen atoms and alkyl groups of the ligand are not shown.

bond lengths are $2.279(1)$ Å for Cu1–P1 and $2.256(1)$ Å for Cu1–P2. For the *closو*-cluster in $1^{N_3}\text{-Cu}(\text{CH}_3\text{CN})_2$, the C–C bond length C1–C2 is $1.808(2)$ Å, while the C–P bonds are C1–P1 = $1.920(2)$ Å and C2–P2 = $1.906(2)$ Å. Similarly to $1^{\text{Cl}}\text{-Cu}(\text{CH}_3\text{CN})_2$, for the *nido*-cluster in $1^{N_3}\text{-Cu}(\text{CH}_3\text{CN})_2$, the carbon–phosphorus bonds are short at $1.786(2)$ Å for C3–P1 and $1.747(2)$ Å for C4–P3. The *nido*-cluster adopts the same C_2 symmetry as in $1^{\text{Cl}}\text{-Cu}(\text{CH}_3\text{CN})_2$, which appears typical for dianionic *nido*- $\{\text{C}_2\text{B}_{10}\}^{2-}$ clusters with two phosphine substituents. The P3–N3 bond length is $1.703(2)$ Å, which is longer than that in the azido-tri(fluoroaryl)phosphonium species $[(\text{HC}_6\text{F}_4)_3\text{P}(\text{N}_3)][\text{B}(\text{C}_6\text{F}_5)_4]$ ($1.651(2)$ Å),⁶⁸ likely due to stabilization by the directly bonded dianionic cluster. The azido fragment slightly deviates from



Data availability

The data supporting this article have been included as part of the SI. CCDC 2453612 (**1**), 2453613 (**1·CuCl**), 2453614 (**1^{Cl}·Cu(CH₃CN)₂**), 2453615 (**1^{N₃}**·Cu(CH₃CN)₂), and 2453616 (**1·CuBPh₄**) contains the supplementary crystallographic data for this paper.^{73–77}

Additional experimental details and crystallographic data. See DOI: <https://doi.org/10.1039/d5sc04058b>.

Acknowledgements

This material is based upon work supported by the National Science Foundation Award CHE-2154828.

Notes and references

- 1 C. A. Tolman, *Chem. Rev.*, 1977, **77**, 313–348.
- 2 V. Lyaskovskyy and B. de Bruin, *ACS Catal.*, 2012, **2**, 270–279.
- 3 J. R. Khusnutdinova and D. Milstein, *Angew. Chem., Int. Ed.*, 2015, **54**, 12236–12273.
- 4 M. T. Whited, *Dalton Trans.*, 2021, **50**, 16443–16450.
- 5 G. Bouhadir and D. Bourissou, *Chem. Soc. Rev.*, 2016, **45**, 1065–1079.
- 6 J. S. Jones and F. P. Gabbaï, *Acc. Chem. Res.*, 2016, **49**, 857–867.
- 7 J. Goodman and S. A. Macgregor, *Coord. Chem. Rev.*, 2010, **254**, 1295–1306.
- 8 A. Tanushi and A. T. Radosevich, *J. Am. Chem. Soc.*, 2018, **140**, 8114–8118.
- 9 G. T. Cleveland and A. T. Radosevich, *Angew. Chem., Int. Ed.*, 2019, **58**, 15005–15009.
- 10 A. J. King and J. M. Goicoechea, *Chem.-Eur. J.*, 2024, **30**, e202400624.
- 11 S. Pavlidis and J. Abbenseth, *Organometallics*, 2025, **44**, 483–486.
- 12 A. D. Ready, Y. A. Nelson, D. F. Torres Pomares and A. M. Spokoyny, *Acc. Chem. Res.*, 2024, **57**, 1310–1324.
- 13 G. B. Gange, A. L. Humphries, D. E. Royzman, M. D. Smith and D. V. Peryshkov, *J. Am. Chem. Soc.*, 2021, **143**, 10842–10846.
- 14 B. C. Nussbaum, C. R. Cavicchi, M. D. Smith, P. J. Pellechia and D. V. Peryshkov, *Inorg. Chem.*, 2024, **63**, 15053–15060.
- 15 H. Wang, J. Zhang, H. K. Lee and Z. Xie, *J. Am. Chem. Soc.*, 2018, **140**, 3888–3891.
- 16 M. Keener, M. Mattejat, S.-L. Zheng, G. Wu, T. W. Hayton and G. Ménard, *Chem. Sci.*, 2022, **13**, 3369–3374.
- 17 E. H. Adillon and J. C. Peters, *J. Am. Chem. Soc.*, 2024, **146**, 30204–30211.
- 18 R. N. Grimes, *Carboranes*, Academic Press, Amsterdam; Boston, 3rd edn, 2016.
- 19 S. P. Fisher, A. W. Tomich, S. O. Lovera, J. F. Kleinsasser, J. Guo, M. J. Asay, H. M. Nelson and V. Lavallo, *Chem. Rev.*, 2019, **119**, 8262–8290.
- 20 M. F. Hawthorne, *Boranes and Beyond: History and the Man Who Created Them*, Springer, New York, NY, 2023.
- 21 A. W. Tomich, J. Chen, V. Carta, J. Guo and V. Lavallo, *ACS Cent. Sci.*, 2024, **10**, 264–271.
- 22 X. Zhang, L. M. Rendina and M. Müllner, *ACS Polym. Au*, 2024, **4**, 7–33.
- 23 M. O. Akram, J. R. Tidwell, J. L. Dutton and C. D. Martin, *Angew. Chem., Int. Ed.*, 2022, **61**, e202212073.
- 24 P. Stockmann, M. Gozzi, R. Kuhnert, M. B. Sárosi and E. Hey-Hawkins, *Chem. Soc. Rev.*, 2019, **48**, 3497–3512.
- 25 Z. Qiu and Z. Xie, *Chem. Soc. Rev.*, 2022, **51**, 3164–3180.
- 26 R. J. Grams, W. L. Santos, I. R. Scorei, A. Abad-García, C. A. Rosenblum, A. Bita, H. Cerecetto, C. Viñas and M. A. Soriano-Ursúa, *Chem. Rev.*, 2024, **124**, 2441–2511.
- 27 A. Weller, *Nat. Chem.*, 2011, **3**, 577–578.
- 28 M. Joost, A. Zeineddine, L. Estévez, S. Mallet-Ladeira, K. Miqueu, A. Amgoune and D. Bourissou, *J. Am. Chem. Soc.*, 2014, **136**, 14654–14657.
- 29 S. P. Fisher, S. G. McArthur, V. Tej, S. E. Lee, A. L. Chan, I. Banda, A. Gregory, K. Berkley, C. Tsay, A. L. Rheingold, G. Guisado-Barrios and V. Lavallo, *J. Am. Chem. Soc.*, 2020, **142**, 251–256.
- 30 J. Schulz, R. Clauss, A. Kazimir, S. Holzknecht and E. Hey-Hawkins, *Angew. Chem., Int. Ed.*, 2023, **62**, e202218648.
- 31 D. Bawari, D. Toami, K. Jaiswal and R. Dobrovetsky, *Nat. Chem.*, 2024, **16**, 1261–1266.
- 32 S. Yao, A. Kostenko, Y. Xiong, A. Ruzicka and M. Driess, *J. Am. Chem. Soc.*, 2020, **142**, 12608–12612.
- 33 M. Keener, C. Hunt, T. G. Carroll, V. Kampel, R. Dobrovetsky, T. W. Hayton and G. Ménard, *Nature*, 2020, **577**, 652–655.
- 34 S. Yao, T. Szilvási, Y. Xiong, C. Lorent, A. Ruzicka and M. Driess, *Angew. Chem., Int. Ed.*, 2020, **59**, 22043–22047.
- 35 B. C. Nussbaum, A. L. Humphries, G. B. Gange and D. V. Peryshkov, *Chem. Commun.*, 2023, **59**, 9918–9928.
- 36 R. Núñez, M. Tarrés, A. Ferrer-Ugalde, F. F. de Biani and F. Teixidor, *Chem. Rev.*, 2016, **116**, 14307–14378.
- 37 J. R. Miller, A. R. Cook, L. Šimková, L. Pospíšil, J. Ludvík and J. Michl, *J. Phys. Chem. B*, 2019, **123**, 9668–9676.
- 38 F. A. Hart, *J. Chem. Soc.*, 1960, 3324–3328.
- 39 J. G. Hartley, L. M. Venanzi and D. C. Goodall, *J. Chem. Soc.*, 1963, 3930–3936.
- 40 Y.-E. Kim, J. Kim and Y. Lee, *Chem. Commun.*, 2014, **50**, 11458–11461.
- 41 W. J. Schreiter, A. R. Monteil, M. A. Peterson, G. T. McCandless, F. R. Fronczek and G. G. Stanley, *Polyhedron*, 2013, **58**, 171–178.
- 42 Z. B. G. Fickenscher, P. Lönncke, A. K. Müller, W. Baumann, B. Kirchner and E. Hey-Hawkins, *Inorg. Chem.*, 2023, **62**, 12750–12761.
- 43 J. Zank, A. Schier and H. Schmidbaur, *J. Chem. Soc., Dalton Trans.*, 1999, 415–420.
- 44 D. J. Schild and J. C. Peters, *ACS Catal.*, 2019, **9**, 4286–4295.
- 45 G. Chakkadabari, Y.-T. Chen, A. J. Karttunen, M. T. Dau, J. Jänis, S. P. Tunik, P.-T. Chou, M.-L. Ho and I. O. Koshevoy, *Inorg. Chem.*, 2016, **55**, 2174–2184.
- 46 W.-C. Shih, W. Gu, M. C. MacInnis, S. D. Timpa, N. Bhuvanesh, J. Zhou and O. V. Ozerov, *J. Am. Chem. Soc.*, 2016, **138**, 2086–2089.



47 B. J. Graziano, M. V. Vollmer and C. C. Lu, *Angew. Chem., Int. Ed.*, 2021, **60**, 15087–15094.

48 V. T. Nguyen, Q. Lai, N. Witayapaisitsan, N. Bhuvanesh, P. Surawatanawong and O. V. Ozerov, *Organometallics*, 2023, **42**, 3120–3129.

49 I.-S. Ke, J. S. Jones and F. P. Gabbaï, *Angew. Chem., Int. Ed.*, 2014, **53**, 2633–2637.

50 C. A. Theulier, Y. García-Rodeja, S. Mallet-Ladeira, K. Miqueu, G. Bouhadir and D. Bourissou, *Organometallics*, 2021, **40**, 2409–2414.

51 M. Sircoglou, N. Saffon, K. Miqueu, G. Bouhadir and D. Bourissou, *Organometallics*, 2013, **32**, 6780–6784.

52 M. P. Boone and D. W. Stephan, *J. Am. Chem. Soc.*, 2013, **135**, 8508–8511.

53 Y.-E. Kim, S. Oh, S. Kim, O. Kim, J. Kim, S. W. Han and Y. Lee, *J. Am. Chem. Soc.*, 2015, **137**, 4280–4283.

54 A. M. Poitras, S. E. Knight, M. W. Bezpalko, B. M. Foxman and C. M. Thomas, *Angew. Chem., Int. Ed.*, 2018, **57**, 1497–1500.

55 A. M. Poitras, M. W. Bezpalko, B. M. Foxman and C. M. Thomas, *Dalton Trans.*, 2019, **48**, 3074–3079.

56 B. M. Gordon, N. Lease, T. J. Emge, F. Hasanayn and A. S. Goldman, *J. Am. Chem. Soc.*, 2022, **144**, 4133–4146.

57 T. Migita, T. Nagai, K. Kiuchi and M. Kosugi, *Bull. Chem. Soc. Jpn.*, 1983, **56**, 2869–2870.

58 D. Marcoux and A. B. Charette, *Adv. Synth. Catal.*, 2008, **350**, 2967–2974.

59 D. Marcoux and A. B. Charette, *J. Org. Chem.*, 2008, **73**, 590–593.

60 M. Duval, C. Blons, S. Mallet-Ladeira, D. Delcroix, L. Magna, H. Olivier-Bourbigou, E. D. S. Carrizo, K. Miqueu, A. Amgoune, G. Szalóki and D. Bourissou, *Dalton Trans.*, 2020, **49**, 13100–13109.

61 H. Kawai, W. J. Wolf, A. G. DiPasquale, M. S. Winston and F. D. Toste, *J. Am. Chem. Soc.*, 2016, **138**, 587–593.

62 Y. H. Lee and B. Morandi, *Coord. Chem. Rev.*, 2019, **386**, 96–118.

63 J. P. H. Charmant, M. F. Haddow, R. Mistry, N. C. Norman, A. G. Orpen and P. G. Pringle, *Dalton Trans.*, 2008, 1409.

64 J. Schulz, A. Kreienbrink, P. Coburger, B. Schwarze, T. Grell, P. Lönnecke and E. Hey-Hawkins, *Chem.-Eur. J.*, 2018, **24**, 6208–6216.

65 Y. O. Wong, M. D. Smith and D. V. Peryshkov, *Chem.-Eur. J.*, 2016, **22**, 6764–6767.

66 Y. O. Wong, M. D. Smith and D. V. Peryshkov, *Chem. Commun.*, 2016, **52**, 12710–12713.

67 A. L. Humphries, G. A. Tellier, M. D. Smith, A. R. Chianese and D. V. Peryshkov, *J. Am. Chem. Soc.*, 2024, **146**, 33159–33168.

68 D. Winkelhaus, M. H. Holthausen, R. Dobrovetsky and D. W. Stephan, *Chem. Sci.*, 2015, **6**, 6367–6372.

69 E. D. Little, S. Bedajna and F. P. Gabbaï, *Chem. Sci.*, 2025, **16**, 10852–10856.

70 H. F. Cheng, A. I. d'Aquino, J. Barroso-Flores and C. A. Mirkin, *J. Am. Chem. Soc.*, 2018, **140**, 14590–14594.

71 J. Mendez-Arroyo, J. Barroso-Flores, A. M. Lifschitz, A. A. Sarjeant, C. L. Stern and C. A. Mirkin, *J. Am. Chem. Soc.*, 2014, **136**, 10340–10348.

72 A. M. Lifschitz, M. S. Rosen, C. M. McGuirk and C. A. Mirkin, *J. Am. Chem. Soc.*, 2015, **137**, 7252–7261.

73 J. R. Riffle, C. L. Jowers, S. Luna, M. D. Smith and D. V. Peryshkov, CCDC 2453612: Experimental CrystalStructure Determination, 2025, DOI: [10.5517/ccdc.csd.cc2nc5s0](https://doi.org/10.5517/ccdc.csd.cc2nc5s0).

74 J. R. Riffle, C. L. Jowers, S. Luna, M. D. Smith and D. V. Peryshkov, CCDC 2453613: Experimental CrystalStructure Determination, 2025, DOI: [10.5517/ccdc.csd.cc2nc5t1](https://doi.org/10.5517/ccdc.csd.cc2nc5t1).

75 J. R. Riffle, C. L. Jowers, S. Luna, M. D. Smith and D. V. Peryshkov, CCDC 2453614: Experimental CrystalStructure Determination, 2025, DOI: [10.5517/ccdc.csd.cc2nc5v2](https://doi.org/10.5517/ccdc.csd.cc2nc5v2).

76 J. R. Riffle, C. L. Jowers, S. Luna, M. D. Smith and D. V. Peryshkov, CCDC 2453615: Experimental CrystalStructure Determination, 2025, DOI: [10.5517/ccdc.csd.cc2nc5w3](https://doi.org/10.5517/ccdc.csd.cc2nc5w3).

77 J. R. Riffle, C. L. Jowers, S. Luna, M. D. Smith and D. V. Peryshkov, CCDC 2453616: Experimental CrystalStructure Determination, 2025, DOI: [10.5517/ccdc.csd.cc2nc5x4](https://doi.org/10.5517/ccdc.csd.cc2nc5x4).

